physica status solidi b pss

www.pss-b.com

Optical Properties of Cubic GaN Quantum Dots Grown by Molecular Beam Epitaxy

Sarah Blumenthal, Dirk Reuter, and Donat J. As*

We have investigated the optical properties of self-assembled cubic GaN quantum dots (QDs) in a cubic AlN matrix grown in Stranski–Krastanov growth mode. Two different sample series are fabricated and optically characterized by photoluminescence measurements. Additionally, the experimental results are compared to theoretical calculations. Sample series A consists of one single QD layer with varying GaN amount. A red shift of emission energy of 140 meV is observed with increasing GaN deposition time. Simulations verify this behavior and can be explained by a decrease of the QD height. Sample series B has two layers of QDs on top of each other with different QD deposition amounts of three and six monolayers, respectively. The spacer layer thickness between the QD layers is 2 and 20 nm. A decreased emission intensity of the smaller QDs is measured for QD layers with smaller spacer layer thickness. This observation is a first hint of an electronic coupling between the two QD layers with thin spacer layer thickness resulting in tunneling of carriers from the smaller QDs to the larger QDs. Theoretical calculations further show that a strain induced structural coupling induces a vertical alignment of the QDs.

1. Introduction

Due to their wide band gap group, III-nitrides are of great interest for future quantum optical and quantum information devices operating in the visible and near-UV range. Especially quantum dots (QDs) are in the focus of research offering narrow optical linewidths due to their reduced dimensionality. For efficient light emitting diodes (LEDs) or laser diodes, the number of active QDs has to be increased as much as possible. Therefore, stacking of QD layers is a promising way to improve the performance of such devices.[1,2] In hexagonal GaN (h-GaN), stacking of QDs resulted in an increase of photoluminescence (PL) intensity.[3] However, in h-GaN a Quantum Confined Stark Effect appears, which is caused by an internal field and leads to a reduced recombination probability.[4] The growth in the metastable zinc blende phase can reduce these internal fields so that no spontaneous polarization fields in (001) growth direction exist.[5] Recently, Bürger et al.[6] have already shown that the growth of c-GaN QDs in Stranski–Krastanov (SK) growth mode leads to QD lifetimes that are about one order of magnitude shorter compared to h-GaN QDs emitting at the same wavelength.[7] Single-photon emission from these QDs[8] as well as the incorporation of QDs into photonic structures, like microdisks and two-dimensional (2D) photonic crystal membranes resulting in high quality factors has also been demonstrated.[9–11] In a previous study, we further reported an increased PL intensity with increasing number of QD layers for cubic GaN QDs embedded in a cubic AlN matrix and transmission electron microscopy (TEM) measurements showed a vertical alignment of the QDs for samples with small spacer layer thicknesses.[12]

In this work, we concentrate on the optical and structural properties of c-GaN QD layers. Therefore, we realized a sample series with one c-GaN QD layer in a c-AlN matrix with varying QD deposition times. The influence of different GaN amounts on the emission energy resulted in a shift of PL emission performed at room temperature. This shift in emission is compared to theoretical calculations of the emission energy as a function of the QD height using the self-consistent Schrödinger–Poisson solver nextnano++.[13]

To study the structural and electrical coupling of QD layers, we fabricated asymmetric QD pairs (AQDP). In these structures, two layers of c-GaN QDs separated by a 2 nm or 20 nm thick c-AlN spacer layer is grown with different deposition amounts in each QD layer. The electrical coupling and non-resonant tunneling is estimated by PL measurements. One important aspect of SK QDs is strain-driven vertical self-organization of island stacks in multilayer samples. Simulations using nextnano++ verify that this mechanism is responsible for the vertical alignment in our cubic GaN QD stacks.

2. Experimental Section

Our samples have been grown by molecular beam epitaxy employing standard effusion cells for the evaporation of gallium and aluminum. The nitrogen is derived from dissociation of N_2 using a plasma cell. The growth is in situ monitored with reflection high energy electron diffraction (RHEED), which allows controlling the 2D growth as well as the formation of QDs.

S. Blumenthal, Dr. D. Reuter, Dr. D. J. As
Department of Physics
University of Paderborn
Warburger Str. 100, 33098 Paderborn, Germany
E-mail: sarah.blumenthal@upb.de

DOI: 10.1002/pssb.201700457

© 2018 WILEY-VCH Verlag GmbH & Co. KGaA, Weinheim

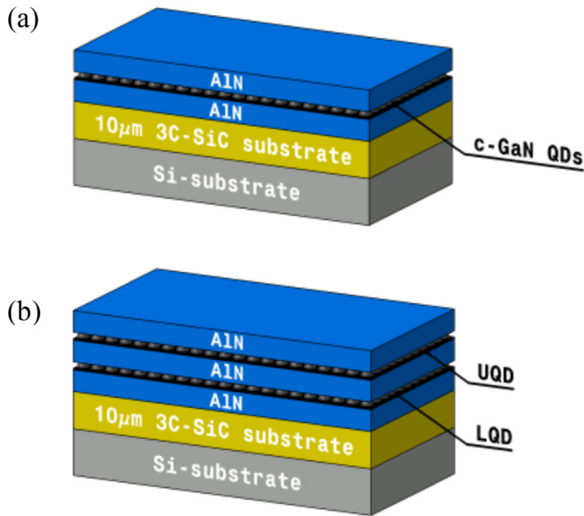

Figure 1. Sample structure of (a) sample series A with one layer of QDs embedded in a c-AlN matrix and (b) sample series B with two layers of QDs with different deposition amounts and a c-AlN in-between.

The growth is performed at a substrate temperature of $T_s = 730\,°C$. More detailed information on the sample growth are provided in Ref. [14]. The substrate consists of a 10 μm thick 3C-SiC layer on top of a 500 μm Si (001) substrate (see **Figure 1**).

Two different sample series are realized. The first series (Figure 1(a)) contains one c-GaN QD layer sandwiched between two 30 nm c-AlN layers. The deposited amount of c-GaN is varied in the sample as described in **Table 1**. The QDs are grown employing the self-assembled SK growth mode caused by a lattice mismatch of 3.2% between c-AlN and c-GaN.[15] After transformation, the QDs and a 3 ML thick wetting layer are formed.

Sample series B (Figure 1(b)) is described in **Table 2**. The samples consist of a 30 nm thick c-AlN buffer layer and a 30 nm thick top layer as well. Two c-GaN QD layers are arranged between the c-AlN matrix. There are disparities in the QD size of the two QD layers (see Table 2). The lower QD layer (LQD), which immediately follows the buffer layer, consists of smaller QDs with a deposition time of $t = 13$ s. The upper QD layer (UQD) is composed of bigger QDs compared to the lower layer having a deposition time of $t = 40$ s. Embedded between the two QD layers a c-AlN spacer layer is realized with different thicknesses of 2 nm and 20 nm, respectively.

Table 1. List of sample series A with one layer of c-GaN QDs embedded in a 60 nm thick c-AlN matrix.

Sample number	c-GaN deposition [s]	c-GaN coverage [ML]
A1	13	3
A2	20	3–4
A3	25	4
A4	30	4–5

Table 2. List of sample series B. The deposition time of LQDs and UQDs and the thickness of the spacer layer is specified.

Sample number	Deposition LQD [s]	Deposition UQD [s]	Thickness spacer layer [nm]
B1	10	40	20
B2	10	40	2

3. Results and Discussion

3.1. Optical Characterization

Photoluminescence measurements of QD samples with one layer of QDs are presented in **Figure 2**. The measurements are performed at room temperature with a Nd:YAG laser at a peak wavelength of 266 nm (energy: 4.66 eV, power: 5 mW, excitation spot diameter: 2 μm). A monochromator with a grating of 300 lines per millimeter and a CCD is used to detect the PL signal. It is worth noting that due to the high band gap of c-AlN of 5.93 eV[16] the excitation energy of the laser is too low to excite carriers in the c-AlN layers. This leads to a direct absorption in the QDs. In addition, the wetting layer of 3 monolayers (ML) can be considered to act like a thin GaN quantum well (QW). Theoretical simulations for such thin QWs resulted in a transition energy of about 5.5 eV, which is also much higher than the used laser energy. Therefore, in our experiments only the QDs are excited.

Figure 2 shows room temperature PL spectra of sample number A1–A4 with different c-GaN deposition times. Each spectrum consists of a superposition of Gaussian shaped emission bands of many individual QDs,[17] which explains the broadening of the peak compared to the delta function-like density of states. The full width half maximum (FWHM) is about 450 meV for sample A1 and about 350 meV for the other samples. The peak intensity of the individual spectra are normalized and they are plotted with an offset in y-direction. A shift to lower energies with increasing c-GaN deposition time is

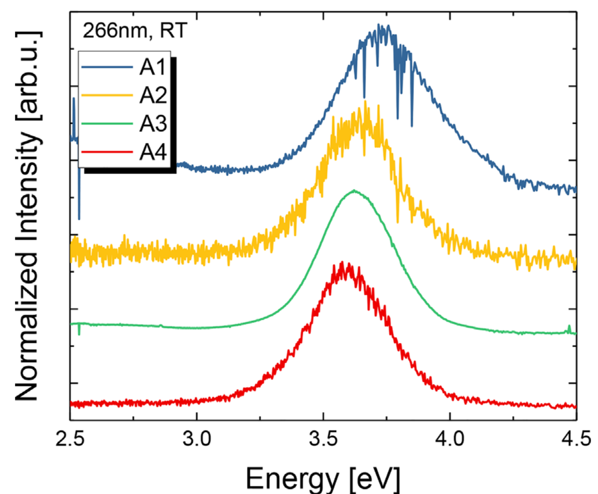

Figure 2. Normalized room temperature PL spectra of one layer of c-GaN QDs with deposition times from 13 s to 30 s. The peak energy is shifted from 3.73 eV to 3.59 eV.

© 2018 WILEY-VCH Verlag GmbH & Co. KGaA, Weinheim

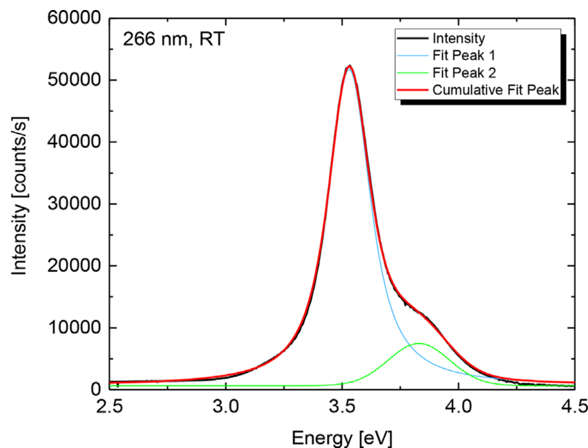

Figure 3. Room temperature PL measurement and corresponding fitting curve of asymmetric QD pairs with a spacer layer thickness of 20 nm (sample number B1). The green line corresponds to the LQDs, the blue line to the UQDs.

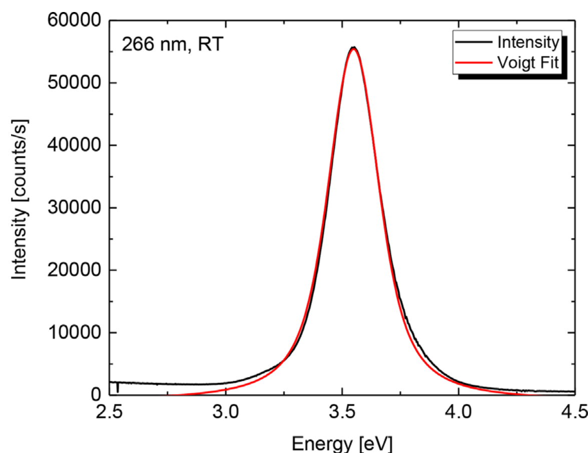

Figure 4. Room temperature PL measurement and corresponding fitting curve of an asymmetric QD pair with a spacer layer thickness of 2 nm (sample number B2).

observed. The redshift covers a range from 3.73 eV (13 s) to 3.59 eV (30 s) leading to a shift of 140 meV. The main confining parameter in our QDs is the QD height.[18] The decrease of the QD emission energy is due to an increase of the QD height.

PL measurements of the QD pairs are shown in **Figures 3 and 4**. The former presents sample number B1 with a spacer layer thickness of $d = 20$ nm. Two peaks can be clearly determined with the help of two Voigt fits (red line shows the cumulative fit). The LQDs (green line) have an emission energy of $E_{LQD} = 3.83$ eV. As expected, the energy of the UQDs is significant lower. In fact, the emission energy is $E_{UQD} = 3.53$ eV, which results in an energy difference of 300 meV. As expected, the emission energies are comparable to the emission energies of the single QD layers of Figure 2.

In contrast to the spectra of the QD pairs with the thicker spacer layer, Figure 4 shows the PL results for sample number B2 with the thinner spacer layer. This spectrum shows only one peak with an emission energy of $E = 3.54$ eV. This emission energy corresponds to the emission of the UQD. It demonstrates an energy difference of 10 meV compared to the single QD layer, which is negligible in comparison to the broad size distribution of the QDs.

In any case, this illustrates that the increase of the spacer layer thickness influences the electronic coupling between the two QD layers. The decreasing emission intensity of the smaller QDs is a first hint of an increasing carrier transfer probability between the two QD layers. This effect is also published for other material systems like InAs/GaAs.[19] They observed that nonresonant tunneling is the microscopic transfer mechanism.

3.2. Nextnano++ Simulations

To investigate the electronic properties of the QDs and to validate the experimental data, simulations are done using nextnano++, a Schrödinger–Poisson solver.[13] The first step needed for the simulations is the implementation of the size, shape, and chemical composition of the 3D QD structure. The QDs are modeled as truncated pyramids with the square bases orientated in the (001) direction and the side facets parallel to the (111) direction (see **Figure 5**). This QD shape was already expected by Fonoberov et al.[18] and experimentally proven by Bürger et al.[6] by TEM measurements. We investigated the transition energies of one single layer as well as the strain of quantum dot pairs. For sample series A with one layer of QDs, the QD height, used for the calculations, varies accordingly to Table 1. Additionally, a wetting layer is implemented with a thickness of about 3 MLs. 1 ML of c-GaN corresponds to $d = 0.225$ nm. The thickness of the wetting layer is also determined in TEM measurements in previous works.[12] For sample series B two layers of QDs, accordingly to Table 2, are realized.

After the modeling of the QDs, nextnano++ continues with solving the strain of the system, followed by iterations of solving the Schrödinger and Poisson equation. The electron and hole wave functions are received using the eight-band k.p model. The band energies are calculated for room temperature.

The parameters used for nextnano++ can be looked up in Ref. [20]. Wecker et al. have shown that the parameters they used fit very well for the calculation of the interband and intraband transitions of c-GaN quantum wells with nextnano3, so we

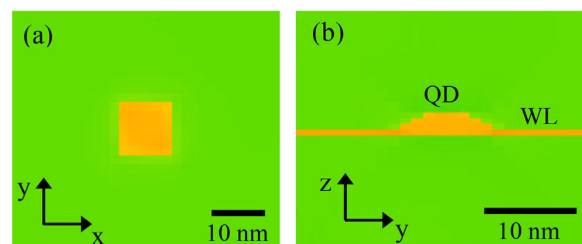

Figure 5. The shape of the QDs simulated with nextnano++. a) In the *x-y*-coordinate system, the bottom of the pyramid is shown. b) The shape shown in the *y-z*-coordinate system. The c-GaN QD has a truncated pyramidal shape. In this case, the QD height is 2 nm and the width of the QD is 10 nm. The wetting layer thickness amounts to 0.7 nm.

© 2018 WILEY-VCH Verlag GmbH & Co. KGaA, Weinheim

expect comparably good results. The additional parameters necessary for eight-band k.p. theory are taken from the material database of nextnano++, where Vurgaftman et al.[21] was the main source.

Figure 5 shows the shape of the quantum dot for one single layer of QDs. The bottom of the pyramid is shown in Figure 5(a) in the *x-y*-coordinate system. Figure 5(b) shows the truncated pyramidal shape in the *y-z*-coordinate system. In this simulation, a wetting layer thickness of 0.7 nm (approximately 3 MLs), a QD width of 10 nm and a QD height of 2 nm is assumed resulting in an aspect ratio of 1:5. For the simulations, the QD height is varied from 0.225 nm to 3 nm to cover a wide range of QD sizes. The WL thickness is kept constant and is not included in the QD height indicated before.

The excitonic properties of the c-GaN QDs are described as a function of the QD height. The simulations are done for three different QD widths. As shown in the measured PL data, the broadening of the emission is large due to the varying of the QD size. For this reason, the simulations are done for a width of 5, 10, and 20 nm, respectively. In **Figure 6**(a), the valence band maximum and the conduction band minimum as a function of the QD height are plotted. The rather slow decrease of the difference between hole and electron energy levels with increasing QD height can be explained by the absence of the piezoelectric field in the cubic phase. For example in wurtzide GaN, the magnitude of the piezoelectric potential increases linearly with increasing the QD height and leads to much smaller energy differences for the higher QDs.[18] It is also visible that the band edges are shifted to higher energies with increasing QD width.

The transition energies plotted versus the QD height are shown in Figure 6(b). The non-existence of the piezoelectric field results not only in a low decrease of the conduction and valence band edges, but also influences the behavior of the emission energy. As a result, the behavior is mainly affected by the deformation potential and confinement.[18] It should be noted that the bulk c-GaN energy gap is at 3.23 eV, which is significantly lower compared to the c-GaN QDs, whereas in the h-GaN the energy drops below the bulk energy caused by the piezoelectric fields.[18]

As already described, due to the SK process the deposited c-GaN amount transforms into a wetting layer and the QDs. Thereby, the wetting layer thickness of about 0.7 nm is much thinner and the QD height is much higher than the deposited amount of GaN. For example, a c-GaN deposition time of 25 s (emission energy $E = 3.62$ eV) leads to a GaN coverage of 4 MLs (0.9 nm). These 4 MLs correspond to the total layer thickness before the layer transforms to a WL and QDs. After the transformation, the simulations show that the same emission energy ($E = 3.62$ eV) results in a QD height of 1.66 nm. This relation is shown in **Figure 7**. The diagram compares the simulated data from Figure 6(b) with the experimental data from Figure 2. The emission energies for the QDs with a width of 10 nm (red line) and 20 nm (green line) are depicted in the plot as a function of the QD height. For the experimental data points (black squares), the GaN coverage determined from the QD deposition amount is plotted versus the peak emission energy. The data fits very well to the experiment. The shapes of the curves are similar. The reason for the deviation of the measured emission energy for the smallest QDs, is that the emission band is about 100 meV broader compared to the others resulting in a much larger error.

Additionally, the influence of QD pairs is investigated theoretically. Therefore, calculations of QD pairs according to sample series B were realized. The results for the strain for the

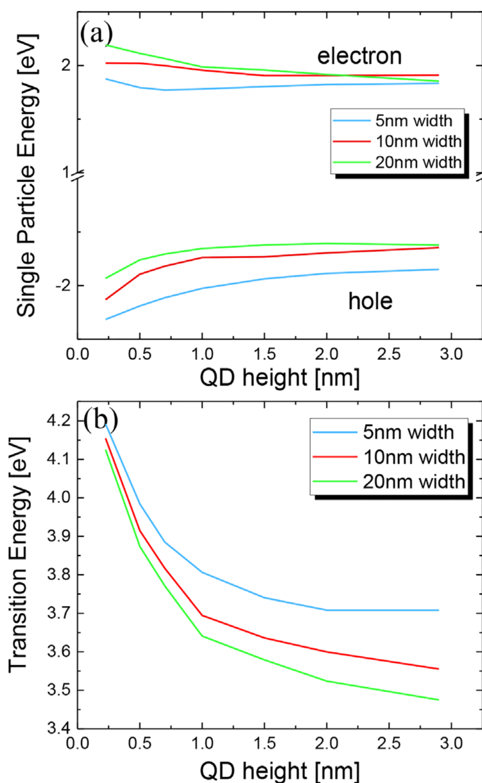

Figure 6. The results of the eight-band k · p model. The diameter of the QD is varied between 5 and 20 nm, because of the broadening of the QD size. a) Conduction band minimum and valence band maximum as a function of the QD height. b) Transition energy as a function of the QD height.

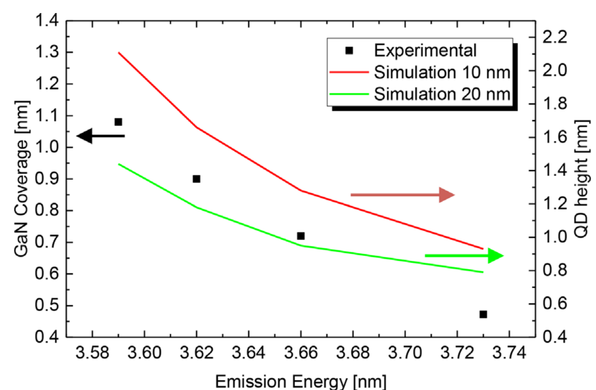

Figure 7. Emission energy as a function of the GaN coverage for the experimental results and the QD height for the simulations for a QD width of 10 and 20 nm.

© 2018 WILEY-VCH Verlag GmbH & Co. KGaA, Weinheim

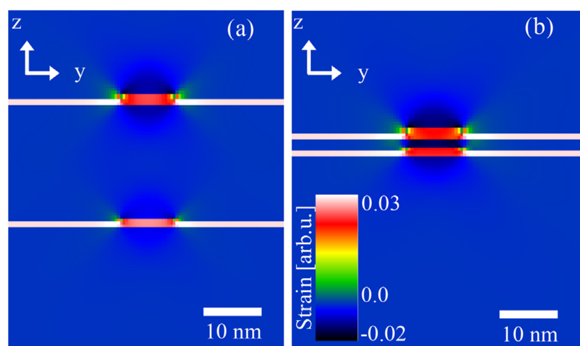

Figure 8. Simulated strain in growth direction for the QD pairs with (a) 20 nm c-AlN spacer layer and (b) 4 nm c-AlN spacer layer.

strain tensor are shown in **Figure 8**, calculated for the component of the strain tensor in the *x*-*y*-plane in growth direction (*z*-direction) for a spacer layer thickness of 20 and 2 nm, respectively. The QD is compressively strained independent of the spacer layer thickness. The strain of the QD also influences its surrounding. Due to this, the c-AlN is tensile strained in this area. It is worth noting, that it is just a coincidence that the QDs in Figure 8(a) are arranged directly on top of each other. If the spacer layer thickness is decreased now (see Figure 8(b)), the tensile strained area in the surrounding of the LQD merges with that of the UQD, resulting in only one huge tensile strained area. This strain induces a vertical alignment of the QD layers with thin spacer layers in-between, which is already shown for c-GaN QDs in Ref. [12] as well as other material systems.[22,23] In the case of a thick spacer layer, the QDs are randomly arranged in each layer. Structural analysis of sample series B need to be performed.

4. Conclusion

We have investigated the optical properties of c-GaN QDs grown by plasma-assisted molecular beam epitaxy on a 10 µm 3C-SiC on top of a Si (001) substrate. The self-assembled c-GaN QDs are grown in SK growth mode in a c-AlN matrix. Sample series A consists of one layer of QDs with varying GaN amount. Sample series B has two layers of QDs with a layer of small LQDs and a layer with big UQDs. The spacer layer in between the QD layers is 2 and 20 nm, respectively. For both sample series, theoretical calculations are compared to the experimental results. PL measurements of the single QD layer show a redshift of emission energy with increasing QD deposition amount. This can be explained by the increase of the QD height, which is the main confining parameter in our QDs. Nextnano++ simulations could successfully verify the emission energies of the single layers.

The PL measurements of the QD pairs give a first hint of an increased carrier transfer probability with decreasing spacer layer thickness. The spectrum of the sample with a thick spacer layer shows two clear emission peaks at 3.83 eV and 3.53 eV corresponding to the UQD and LQD. These emission energies fit very well to the emission energies of the single QD layer. A decrease of the spacer layer thickness leads to a disappearance of the emission of the LQD, so that only one single emission peak is observed at 3.54 eV, which corresponds to the UQD layer. This suggests an electrical coupling of the QD layers with thin spacer layer thickness. Additionally, strain calculations with nextnano++ software are realized to prove a structural coupling between the QD layers with thin spacer layer thickness. The QDs are compressively strained in growth direction. This strain influences the surrounding of the QDs and leads to a tensile strained c-AlN. With decreasing spacer layer thickness, the strain of the LQD influences the UQD and induces a vertical alignment of the QD.

Acknowledgements

This work was financially supported by the DFG graduate program GRK 1464 “Micro- and Nanostructures in Optoelectronics and Photonics” and the Collaborative Research Centre TRR 142 “Tailored nonlinear photonics: From fundamental concepts to functional structures” (Project B02).

Conflicts of Interest

The authors declare no conflicts of interest.

Keywords

cubic crystals, GaN, molecular beam epitaxy, optical properties, quantum dots

Received: August 24, 2017
Revised: November 20, 2017
Published online: January 24, 2018

[1] H. Saito, K. Nishi, I. Ogura, S. Sugou, Y. Sugimoto, *Appl. Phys. Lett.* **1996**, *69*, 3140.
[2] M. V. Maximov, Y. M. Shemyakov, A. F. Tsatsul'nikov, A. V. Lunev, A. V. Sakharov, V. M. Ustinov, A. Y. Egerov, A. E. Zhukov, A. R. Kovsh, P. S. Kop'ev, L. V. Asryan, Z. I. Alferov, N. N. Ledentsov, D. Bimberg, A. O. Kosogov, P. Werner, *J. Appl. Phys.* **1998**, *83*, 5561.
[3] K. Hoshino, S. Kako, Y. Arakawa, *Phys. Status Solidi B* **2003**, *240*, 322.
[4] C. Santori, S. Götzinger, Y. Yamamoto, *Appl. Phys. Lett.* **2005**, *87*, 051916.
[5] T. Schupp, T. Meisch, B. Neuschl, M. Feneberg, K. Thonke, K. Lischka, D. J. As, *Phys. Status Solidi C* **2011**, *8*, 1495.
[6] M. Bürger, J. K. N. Lindner, D. Reuter, D. J. As, *Phys. Status Solidi C* **2015**, *12*, 452.
[7] S. Kako, M. Miyamura, K. Tachibana, K. Hoshino, Y. Arakawa, *Appl. Phys. Lett.* **2003**, *83*, 984.
[8] S. Kako, M. Holmes, S. Sergent, M. Bürger, D. J. As, Y. Arakawa, *Appl. Phys. Lett.* **2014**, *104*, 011101.
[9] M. Bürger, M. Ruth, S. Declair, J. Förstner, C. Meier, D. J. As, *Appl. Phys. Lett.* **2013**, *102*, 081105.
[10] S. Blumenthal, M. Bürger, A. Hildebrandt, J. Förstner, N. Weber, C. Meier, D. Reuter, D. J. As, *Phys. Status Solidi C* **2016**, *13*, 292.
[11] S. Sergent, S. Kako, M. Bürger, S. Blumenthal, K. Tanabe, S. Iwamoto, D. J. As, Y. Arakawa, *Appl. Phys. Express* **2016**, *9*, 012002.
[12] S. Blumenthal, T. Rieger, D. Meertens, A. Pawlis, D. Reuter, D. J. As, *Phys. Status Solidi B* **2017**, *254*, 1600729.

© 2018 WILEY-VCH Verlag GmbH & Co. KGaA, Weinheim

[13] S. Birner, S. Hackenbuchner, M. Sabathil, G. Zandler, J. A. Majewski, T. Andlauer, T. Zibold, R. Morschl, A. Trellakis, P. Vogl, *Acta Phys. Polon. A* **2006**, *110*, 111.
[14] T. Schupp, T. Meisch, B. Neuschl, M. Feneberg, K. Thonke, K. Lischka, D. J. As, *AIP Conf. Proc*. **2010**, *1292*, 165.
[15] S. Strite, J. Ruan, Z. Li, A. Salvador, H. Chen, D. J. Smith, W. J. Choyke, H. Morkoc, *J. Vac. Sci. Technol. B* **1991**, *9*, 1924.
[16] M. Röppischer, R. Goldhahn, G. Rossbach, P. Schley, C. Cobet, N. Esser, T. Schupp, K. Lischka, D. J. As, *J. Appl. Phys*. **2009**, *106*, 076104.
[17] S. Sergent, S. Kako, M. Bürger, D. J. As, Y. Arakawa, *Appl. Phys. Lett*. **2013**, *103*, 151109.
[18] V. A. Fonoberov, A. A. Balandin, *J. Appl. Phys*. **2003**, *94*, 7178.
[19] R. Heitz, I. Mukhametzhanov, P. Chen, A. Madhukar, *Phys. Rev. B* **1998**, *58*, 10151.
[20] T. Wecker, F. Hörich, M. Feneberg, R. Goldhahn, D. Reuter, D. J. As, *Phys. Status Solidi B* **2015**, *252*, 873.
[21] I. Vurgaftman, J. R. Meyer, *J. Appl. Phys*. **2003**, *94*, 3675.
[22] G. S. Solomon, J. A. Trezza, A. F. Marshall, J. S. Harris, Jr., *Phys. Rev. Lett*. **1996**, *6*, 952.
[23] N. N. Ledentsov, V. A. Shchukin, M. Grundmann, N. Kirstaedter, J. Böhrer, O. Schmidt, D. Bimberg, V. M. Ustinov, A. Yu. Egorov, A. E. Zhukov, P. S. Kop'ev, S. V. Zaitsev, N. Yu. Gordeev, Zh. I. Alferov, A. I. Borovkov, A. O. Kosogov, S. S. Ruvimov, P. Werner, U. Gösele, J. Heydenreich, *Phys. Rev. B* **1996**, *54*, 8743.

© 2018 WILEY-VCH Verlag GmbH & Co. KGaA, Weinheim